Dynamic Dissipative Cooling of a Mechanical Resonator in Strong Coupling Optomechanics

Yong-Chun Liu,[1,2] Yun-Feng Xiao,[1,*] Xingsheng Luan,[2] and Chee Wei Wong[2,†]

[1]State Key Laboratory for Mesoscopic Physics and School of Physics, Peking University, Beijing 100871, People's Republic of China
[2]Optical Nanostructures Laboratory, Columbia University, New York, New York 10027, USA

(Received 27 December 2012; published 12 April 2013)

Cooling of mesoscopic mechanical resonators represents a primary concern in cavity optomechanics. In this Letter, in the strong optomechanical coupling regime, we propose to dynamically control the cavity dissipation, which is able to significantly accelerate the cooling process while strongly suppressing the heating noise. Furthermore, the dynamic control is capable of overcoming quantum backaction and reducing the cooling limit by several orders of magnitude. The dynamic dissipation control provides new insights for tailoring the optomechanical interaction and offers the prospect of exploring mesoscopic quantum physics.

DOI: 10.1103/PhysRevLett.110.153606 PACS numbers: 42.50.Wk, 07.10.Cm, 42.50.Lc

One of the ultimate goals in quantum physics is to overcome thermal noise, so that quantum effects can be observed experimentally. A prominent example is cavity optomechanics [1,2], which enables not only the fundamental test of quantum theory and the exploration of the quantum-classical boundary but also important applications in quantum information processing and precision metrology. For these applications, the first crucial step is to prepare the mechanical resonator in the quantum regime [3–5]. So far, numerous experiments have focused on backaction cooling [6–12] in the weak optomechanical coupling regime, offering the potential for ground-state preparation of mechanical resonators in the resolved sideband condition [13–15], along with backaction evading quantum nondemolition measurements [16–19]. A further step lies in strong coupling, essential for coherent quantum optomechanical manipulations [5,20–24] and electromechanical interactions [25,26]. However, to date, optomechanical cooling in the strong coupling regime has predicted only limited improvement over weak coupling due to the saturation effect of the steady-state cooling rate [22,27,28]. Although strong coupling allows state swapping [5,21], it cools the mechanical resonator only at a single instant in the Rabi oscillation cycle. Thus it is urgent that these limitations for cooling and manipulating mesoscopic mechanical systems in the quantum regime be overcome.

For this purpose, in this Letter we show the dynamic tailoring of the cooling and heating processes by exploiting the cavity dissipation, overcoming the saturation of the steady-state cooling rate. This greatly accelerates the cooling process and thereby strongly suppresses the thermal noise. Moreover, heating induced by swapping and interaction quantum backaction are largely suppressed by periodic modulation of the cavity dissipation, which breaks the fundamental limitation of backaction cooling.

We consider a generic optomechanical system in which an optical cavity driven by a laser is coupled to a mechanical resonance mode, as illustrated in Fig. 1(a). In the rotating frame at the driven laser frequency ω, the system Hamiltonian reads $H = -(\omega - \omega_c)a^\dagger a + \omega_m b^\dagger b + g a^\dagger a(b + b^\dagger) + (\Omega a^\dagger + \Omega^* a)$ [29], where a (b) represents the annihilation operator for the optical (mechanical) mode with ω_c (ω_m) being the corresponding angular resonance frequency; g denotes the single-photon optomechanical coupling rate, and Ω represents the driving strength. For strong driving, the Hamiltonian can be linearized, with $a \equiv a_1 + \alpha$, $b \equiv b_1 + \beta$. Here a_1 and b_1 describe the fluctuations around the mean values $\alpha \equiv \langle a \rangle$ and $\beta \equiv \langle b \rangle$, respectively. Neglecting the nonlinear terms, this yields the Hamiltonian

$$H_L = -\Delta' a_1^\dagger a_1 + \omega_m b_1^\dagger b_1 + (G a_1^\dagger + G^* a_1)(b_1 + b_1^\dagger), \tag{1}$$

where $\Delta' = \omega - \omega_c + 2|G|^2/\omega_m$ is the optomechanical-coupling modified detuning, and $G = \alpha g$ describes the linear coupling strength. Taking the dissipations into consideration, the system is governed by the quantum master equation $\dot{\rho} = i[\rho, H_L] + \kappa \mathcal{D}[a_1]\rho + \gamma(n_{\rm th} + 1)\mathcal{D}[b_1]\rho + \gamma n_{\rm th}\mathcal{D}[b_1^\dagger]\rho$, where $\mathcal{D}[\hat{o}]\rho = \hat{o}\rho\hat{o}^\dagger - (\hat{o}^\dagger\hat{o}\rho + \rho\hat{o}^\dagger\hat{o})/2$ denotes the Liouvillian in Lindblad form for operator $\hat{o}$; $\kappa \equiv \omega_c/Q_c$ ($\gamma \equiv \omega_m/Q_m$) represents the dissipation rate

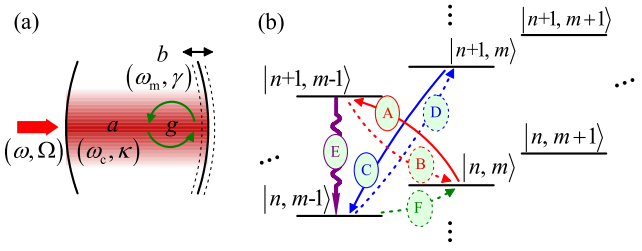

FIG. 1 (color online). (a) Sketch of a typical optomechanical system. (b) Level diagram of the linearized Hamiltonian [Eq. (1)]. $|n, m\rangle$ denotes the state of n photons and m phonons in the displaced frame. The solid (dashed) curves with arrows correspond to the cooling (heating) processes.

of the optical cavity (mechanical) mode, and $n_{\rm th} = 1/(e^{\hbar\omega_m/k_B T} - 1)$ corresponds to the thermal phonon number at the environmental temperature T.

Figure 1(b) displays the level diagram of H_L and the coupling routes among states $|n, m\rangle$ with n (m) being the photon (phonon) number in the displaced frame. We note that there are three kinds of heating processes denoted by the dashed curves in Fig. 1(b), corresponding to swap heating (B), quantum backaction heating (D), and thermal heating (F). Suppressing thermal heating is the ultimate goal while swap heating and quantum backaction heating are the accompanying effect when radiation pressure is utilized to cool the mechanical motion. Swap heating emerges when the system is in the strong coupling regime which enables reversible energy exchange between photons and phonons. Meanwhile, quantum backaction heating can pose a fundamental limit for backaction cooling. The solid curves (A, C, and E) illustrate cooling processes associated with energy swapping, counter-rotating-wave interaction, and cavity dissipation, which one seeks to enhance while suppressing heating for efficient mechanical motion cooling.

We focus on the resolved sideband regime $\kappa < \omega_m$ and we set $\Delta' = -\omega_m$, in which the beam splitter interaction $a_1^\dagger b_1 + a_1 b_1^\dagger$ is on resonance. In this case the dynamical stability condition from the Routh-Hurwitz criterion [30] requires $2|G| < \omega_m$. To realize cooling, the cooperativity $C \equiv 4|G|^2/(\gamma\kappa) \gg 1$ should also be satisfied. Starting from the master equation, we obtain a set of differential equations for the mean values of the second-order moments $\bar{N}_a = \langle a_1^\dagger a_1\rangle$, $\bar{N}_b = \langle b_1^\dagger b_1\rangle$, $\langle a_1^\dagger b_1\rangle$, $\langle a_1 b_1\rangle$, $\langle a_1^2\rangle$, and $\langle b_1^2\rangle$ (see the Supplemental Material [31]). In the steady state we obtain the phonon occupancy [22,27]

$$\bar{N}_{\rm std} \simeq \frac{\gamma(4|G|^2 + \kappa^2)}{4|G|^2(\kappa + \gamma)} n_{\rm th} + \frac{\kappa^2 + 8|G|^2}{16(\omega_m^2 - 4|G|^2)}, \quad (2)$$

where the first term is the classical cooling limit and the second term originates from the quantum backaction, consisting of both dissipation quantum backaction related to the cavity dissipation (with the associated fluctuation-dissipation theorem) and interaction quantum backaction associated with the optomechanical interaction (see the Supplemental Material [31] for a full description). In the weak coupling regime, Eq. (2) reduces to $\bar{N}_{\rm std}^{\rm wk} \simeq \gamma n_{\rm th}/(\Gamma + \gamma) + \kappa^2/(16\omega_m^2)$ with $\Gamma = 4|G|^2/\kappa$, which agrees with Refs. [13,14], and with $\kappa^2/(16\omega_m^2)$ the dissipation quantum backaction from the fluctuation-dissipation theorem. In the strong coupling regime, we obtain $\bar{N}_{\rm std}^{\rm str} \simeq \gamma n_{\rm th}/(\kappa + \gamma) + |G|^2/[2(\omega_m^2 - 4|G|^2)]$. In this case the classical limit is restricted by the cavity dissipation rate κ, while the interaction quantum backaction limit suffers from the high coupling rate $|G|$.

To study the cooling dynamics beyond the steady state, we solve the differential equations to obtain the time evolution of the mean phonon number $\bar{N}_b$. For weak coupling, we have $\bar{N}_b^{\rm wk} \simeq n_{\rm th}(\gamma + \Gamma e^{-\Gamma t})/(\gamma + \Gamma) + [\kappa^2/(16\omega_m^2)](1 - e^{-\Gamma t})$, which shows that the mean phonon number decays exponentially with the cooling rate Γ. This cooling rate is limited by the coupling strength, since in the cooling route $A \rightarrow E$ the energy flow from the mechanical mode to the optical mode (process A) is slower than the cavity dissipation (process E).

In the strong coupling regime, we obtain the time evolution of the mean phonon number described by (see the Supplemental Material [31])

$$\begin{aligned}
&\bar{N}_b^{\rm str} = \bar{N}_{b,1}^{\rm str} + \bar{N}_{b,2}^{\rm str},\\
&\bar{N}_{b,1}^{\rm str} \simeq n_{\rm th}\frac{\gamma + \frac{1}{2}e^{-(\kappa+\gamma)t/2}[\kappa - \gamma + (\kappa+\gamma)\cos(\omega_+ - \omega_-)t]}{\kappa + \gamma},\\
&\bar{N}_{b,2}^{\rm str} \simeq \frac{|G|^2[1 - e^{-(\kappa+\gamma)t/2}\cos(\omega_+ + \omega_-)t\cos(\omega_+ - \omega_-)t]}{2(\omega_m^2 - 4|G|^2)},
\end{aligned} \quad (3)$$

where $\omega_\pm = \sqrt{\omega_m^2 \pm 2|G|\omega_m}$ are the normal eigenmode frequencies. The phonon occupancy exhibits oscillation under an exponentially decaying envelope and can be divided into two distinguished parts $\bar{N}_{b,1}^{\rm str}$ and $\bar{N}_{b,2}^{\rm str}$, where the first part originates from energy exchange between optical and mechanical modes, and the second part is induced by quantum backaction. $\bar{N}_{b,1}^{\rm str}$ reveals the Rabi oscillation with frequency $\sim 2|G|$, whereas the envelopes have the same exponential decay rate $\Gamma' = (\kappa + \gamma)/2$ regardless of the coupling strength $|G|$. This is because, in the strong coupling regime, the cooling route $A \rightarrow E$ is subjected to the cavity dissipation (process E), which has a slower rate than the energy exchange between phonons and photons (process A). This saturation prevents a higher cooling speed for stronger coupling. In Figs. 2(a) and 2(b) we plot the numerical results based on the master equation for various G. It shows that for weak coupling the cooling rate increases rapidly as the coupling strength increases, whereas for strong coupling the envelope decay no longer increases; instead the oscillation frequency becomes larger.

Fast cooling to the steady-state limit.—To speed up the cooling process in the strong coupling regime, here we take advantage of high cavity dissipation to dynamically strengthen the cooling process E. The internal cavity dissipation is abruptly increased each time the Rabi oscillation reaches a minimum-phonon state, such as through rf-synchronized carrier injection to the optical cavity [32]. At this time the system has transited from state $|n, m\rangle$ to state $|n + 1, m - 1\rangle$. Once a strong dissipation pulse is applied to the cavity so that process E dominates, the system will irreversibly transit from state $|n + 1, m - 1\rangle$ to state $|n, m - 1\rangle$ [Fig. 1(b)]. The dissipation pulse essentially behaves as a switch to halt the reversible Rabi oscillation, resulting in the suppression of swap heating. To verify this dissipative cooling, in Figs. 2(c) and 2(d) we plot the modulation scheme and the corresponding time evolution of the mean phonon number $\bar{N}_b$ for $\kappa/\omega_m = 0.05$ and

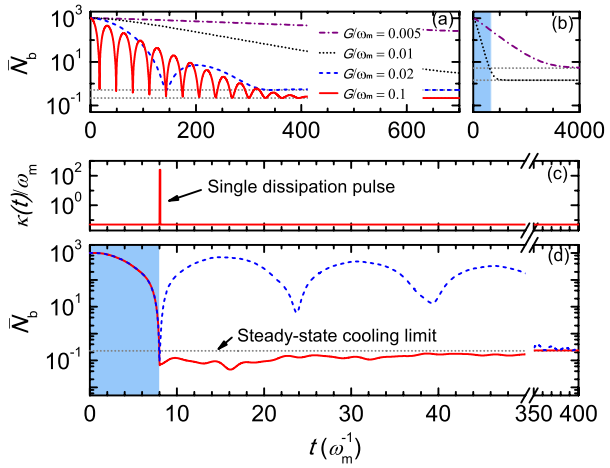

FIG. 2 (color online). (a) Time evolution of mean phonon number $\bar{N}_b$ for $G/\omega_m = 0.005$, 0.01, 0.02, and 0.1 (numerical results). (b) $\bar{N}_b$ for $G/\omega_m = 0.005$ and 0.01 with a wider time interval. The shadowed region shows the same time interval with (a). (c) Modulation scheme of the cavity dissipation rate $\kappa(t)$ for fast cooling to the steady-state limit and (d) the time evolution of mean phonon number $\bar{N}_b$ with (red solid curve) and without (blue dashed curve) modulation for $G/\omega_m = 0.2$. Other parameters are $n_{\rm th} = 10^3$, $\gamma/\omega_m = 10^{-5}$, and $\kappa/\omega_m = 0.05$. The dotted horizontal lines correspond to the steady-state cooling limits, given by Eq. (2).

$G/\omega_m = 0.2$. At the end of the first half Rabi oscillation cycle $t \sim \pi/(2|G|)$, a dissipation pulse of pulse width $0.01\pi/(2|G|)$ is applied. Detailed tradeoffs of the dissipation quantum backaction and the interaction quantum backaction for varying pulse widths are shown in the Supplemental Material [31]. After incidence of the dissipation pulse, the phonon number reaches and remains near the steady-state limit. For short time scales, the remaining small-amplitude oscillations mainly originate from counter-rotating-wave interactions. Note that without modulation (blue dashed curve), the steady-state cooling limit is reached only after $t \simeq 400/\omega_m$; while with the modulation (red solid curve), it only takes $t \simeq 8/\omega_m$ to cool below the same limit.

Breaking the fundamental limit of backaction cooling.— By periodically modulating the cavity dissipation so as to continuously suppress the swap heating, the phonon occupancy can be kept below the steady-state cooling limit. Actually, each time after the dissipation pulse is applied, the photon number quickly drops to the vacuum state, which equivalently reinitializes the system. By periodic pulse application, the system will periodically reinitialize, which keeps the phonon occupancy in an instantaneous-state cooling limit as verified in Fig. 3. The instantaneous-state cooling limit is given by (see the Supplemental Material [31])

$$\bar{N}_{\rm ins} \simeq \frac{\pi\gamma n_{\rm th}}{4|G|} + \frac{\pi^2|G|^4}{(\omega_m^2 - |G|^2)(\omega_m^2 - 4|G|^2)}. \quad (4)$$

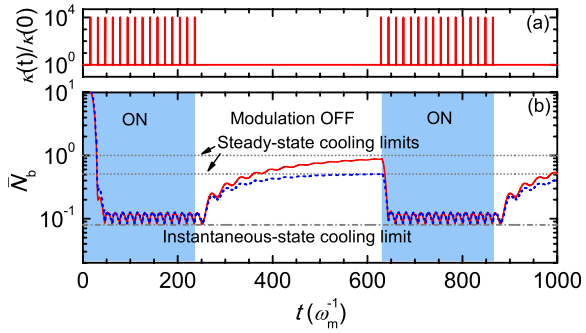

FIG. 3 (color online). Modulation scheme of $\kappa(t)/\kappa(0)$ (a) and the corresponding time evolution of $\bar{N}_b$ (b) for $G/\omega_m = 0.1$, $\kappa(0)/\omega_m = 0.01$ (red solid curve) and 0.02 (blue dashed curve). In (b), the two dotted horizontal lines (from top to bottom) denote the respective steady-state cooling limits depending on the cavity decay $\kappa(0)$, given by Eq. (2); the dash-dotted line denotes the instantaneous-state cooling limit independent of $\kappa(0)$, given by Eq. (4); the "ON" and "OFF" regions correspond to the modulation turned on and off, respectively; the vertical coordinate range from 10 to 10^3 is not shown. Other parameters are $n_{\rm th} = 10^3$ and $\gamma/\omega_m = 10^{-5}$.

Here the first term comes from $\bar{N}_{b,1}^{\rm str}$ for $t \simeq \pi/(2|G|)$, which reduces the steady-sate cooling limit by a factor of $\pi\kappa/(4|G|)$. The second term of $\sim\pi^2|G|^4/\omega_m^4$, obtained from $\bar{N}_{b,2}^{\rm str}$ when $t \simeq \pi/\omega_m$, reveals that the second-order term of $|G|/\omega_m$ in quantum backaction has been removed in our approach, leaving only the higher-order terms. Note that the cooling limit [Eq. (4)] is the sum of the individual minimum of $\bar{N}_{b,1}^{\rm str}$ and $\bar{N}_{b,2}^{\rm str}$ in their first oscillation cycle. Notably, in Fig. 3 we demonstrate that the modulation is switchable. If we turn on the modulation ("ON" region), the system will reach the instantaneous-state cooling limit; if we turn off the modulation ("OFF" region), the system transits back to the steady-state cooling limit.

In particular, from Eq. (3), the interaction quantum backaction heating term $\bar{N}_{b,2}^{\rm str}$ forms a carrier-envelope type evolution, where the carrier oscillation represents the counter-rotating-wave interaction and the envelope oscillation is a result of coherent energy exchange due to strong coupling. The minimum of $\bar{N}_{b,2}^{\rm str}$ is dependent on the carrier-envelope frequency matching. If $(\omega_+ + \omega_-)/(\omega_+ - \omega_-) = k$ $(k = 3, 5, \ldots)$, yielding $|G|/\omega_m = k/(k^2+1) = 0.3,\ 5/26, \ldots,$ $\bar{N}_{b,2}^{\rm str}$ reaches a minimum $\sim\frac{\pi\kappa|G|}{8(\omega_m^2 - 4|G|^2)}$ for $t \simeq \pi/(2|G|)$. Here we obtain the optimized instantaneous-state cooling limit as [31]

$$\bar{N}_{\rm ins}^{\rm opt} \simeq \frac{\pi\kappa}{4|G|}\left[\frac{\gamma n_{\rm th}}{\kappa} + \frac{|G|^2}{2(\omega_m^2 - 4|G|^2)}\right], \quad (5)$$

which reduces both the classical and quantum steady-state cooling limits by a factor of $\pi\kappa/(4|G|)$. Remarkably, this reduction is significant when the system is in the deep strong coupling regime. Besides, the leading order of the interaction quantum backaction heating scales as

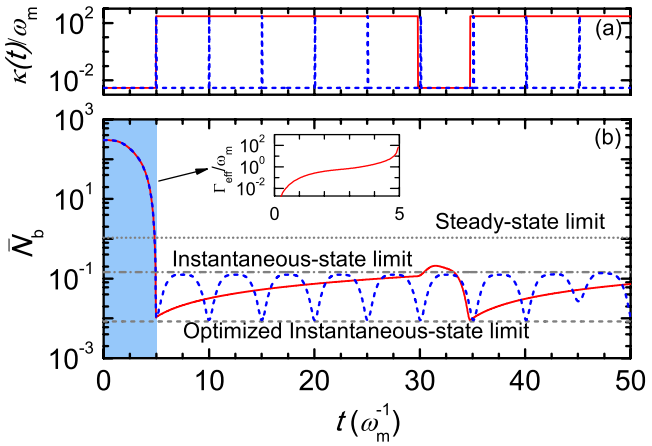

FIG. 4 (color online). Different pulse widths (a) and the corresponding time evolution (b) of $\bar{N}_b$. The horizontal lines indicate the three cooling limits given by Eqs. (2), (4), and (5), from top to bottom. The inset shows the effective cooling rate as a function of time. Parameters are $n_{\rm th} = 300$, $G/\omega_m = 0.3$, $\kappa/\omega_m = 0.003$, and $\gamma/\omega_m = 10^{-5}$.

$\kappa|G|/\omega_m^2$, which can be a few orders of magnitude lower than the steady-state case, representing a large suppression of quantum backaction.

To verify suppression of the interaction quantum backaction heating, in Fig. 4 we plot the cooling dynamics with dissipation modulation for $G/\omega_m = 0.3$ and $\kappa/\omega_m = 0.003$. The single modulation pulse brings down the phonon occupation to the optimized instantaneous-state cooling limit described in Eq. (5), with the time-dependent effective cooling rate $\Gamma_{\rm eff} = (d\bar{N}_b/dt)/\bar{N}_b$ shown in the inset. With short-pulse modulation (blue dashed curve), the remaining oscillation, mainly induced by the counter-rotating-wave interaction, has a quasiperiod of $\pi/(2|G|)$ due to frequency matching. This small-amplitude fluctuation around the instantaneous-state cooling limit might affect future quantum protocols, but in the sense of time averaging through time scales larger than $\pi/(2|G|)$, the cooling limit can be viewed as stable. By using long-pulse modulation, the quasiperiodic fluctuations can be suppressed (red solid curve). This is because the large dissipation suppresses the interaction quantum backaction. The cost is that the dissipation quantum backaction takes effect and gradually increases the phonon number. This tradeoff can be balanced by optimizing the pulse width as shown in the Supplemental Material [31].

Figure 5 plots the cooling limits as functions of G/ω_m, which reveals that instantaneous-state cooling limits are much lower than steady-state cooling limits. For small coupling rates, we observed that interaction quantum backaction is insignificant and suppression of swap heating is the main origin of cooling limit reduction. For large coupling rates, suppressing interaction quantum backaction is crucial for obtaining lower limits. Typically, the cooling limits can be reduced by a few orders of magnitude. For

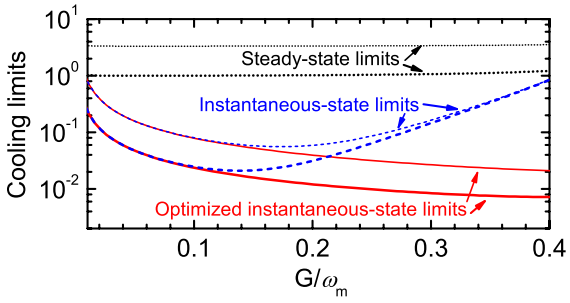

FIG. 5 (color online). Cooling limits given by Eqs. (2) (black dotted curves), (4) (blue dashed curves), and (5) (red solid curves) versus G/ω_m for $n_{\rm th} = 10^3$ (thin curves), 3×10^2 (thick curves). Other parameters are $\kappa/\omega_m = 0.003$ and $\gamma/\omega_m = 10^{-5}$.

example, when $G/\omega_m = 0.3$ and $\kappa/\omega_m = 0.003$, we obtain $\bar{N}_{\rm std} = 3.4$, while $\bar{N}_{\rm ins}^{\rm opt} = 0.03$, corresponding to a phonon number suppression of more than 100 times.

Experimentally, the dynamic control of cavity dissipation can be realized, for example, by modulating the free-carrier plasma density [32–34] or using a light absorber or scatterer [35]. Note that we assume that G is kept unchanged when the dissipation pulses are applied, which corresponds to the invariableness of the intracavity field α. This can be fulfilled by simultaneously changing the driving $\Omega(t)$, so that the equation $[i\Delta' - \kappa(t)/2]\alpha - i\Omega(t) = 0$ is satisfied all the time (see Section VI of the Supplemental Material [31]). Here modulated square-shaped dissipation pulses are used and further simulations show that the results are irrespective of the pulse shape, as long as they are executed quickly with a strong enough peak value at the desired time. This is because the pulse dissipation mainly relies on the pulse area.

In summary, we examined cooling of mesoscopic mechanical resonators in the strong coupling regime and propose dynamic dissipative schemes which possess large cooling rates, low cooling limits, and long-time stability. By making use of the cavity dissipation, swap heating can be strongly avoided and the interaction quantum backaction is largely suppressed, with great advantages over the current conventional cooling approaches. For example, a single dissipation pulse enables a more than 50 times higher cooling rate; with periodic modulation of cavity dissipation, the cooling limit can be reduced by more than 2 orders of magnitude. Unlike the cooling schemes with modulated coupling [36–40], we take advantage of large cavity dissipation, usually regarded as a noise source. Together with recent proposals of other dissipative effects such as two-level ensembles [41] or the photothermal effect [42,43], we demonstrate that cavity dissipation (even in the presence of the considered dissipation quantum backaction) can be viewed as a resource. Compared with the dissipative coupling [44–46], this active dissipation control does not require coupling between the cavity

dissipation and the mechanical resonator. The dynamic dissipative cooling provides a new way for exploring the quantum regime of mechanical devices, ranging from mechanical ground state preparation to generation of mesoscopic quantum states and quantum-limited measurements.

We thank H.-K. Li for discussions. This work is supported by the DARPA ORCHID program (C11L10831), the 973 program (2013CB328704, 2013CB921904), NSFC (11004003, 11222440, and 11121091), and RFDPH (20120001110068). Y.-C. L is supported by the Ph.D. Students' Short-term Overseas Research Program of Peking University and Scholarship Award for Excellent Doctoral Students granted by the Ministry of Education.

*Corresponding author.
yfxiao@pku.edu.cn; http://www.phy.pku.edu.cn/~yfxiao/index.html
†Corresponding author.
cww2014@columbia.edu

[1] T. J. Kippenberg and K. J. Vahala, Science **321**, 1172 (2008).
[2] F. Marquardt and S. M. Girvin, Physics **2**, 40 (2009).
[3] J. D. Teufel, T. Donner, D. Li, J. W. Harlow, M. S. Allman, K. Cicak, A. J. Sirois, J. D. Whittaker, K. W. Lehnert, and R. W. Simmonds, Nature (London) **475**, 359 (2011).
[4] J. Chan, T. P. Mayer Alegre, A. H. Safavi-Naeini, J. T. Hill, A. Krause, S. Gröblacher, M. Aspelmeyer, and O. Painter, Nature (London) **478**, 89 (2011).
[5] E. Verhagen, S. Deléglise, S. Weis, A. Schliesser, and T. J. Kippenberg, Nature (London) **482**, 63 (2012).
[6] S. Gigan, H. R. Böhm, M. Paternostro, F. Blaser, G. Langer, J. B. Hertzberg, K. C. Schwab, D. Bäuerle, M. Aspelmeyer, and A. Zeilinger, Nature (London) **444**, 67 (2006).
[7] O. Arcizet, P.-F. Cohadon, T. Briant, M. Pinard, and A. Heidmann, Nature (London) **444**, 71 (2006).
[8] A. Schliesser, R. Rivière, G. Anetsberger, O. Arcizet, and T. J. Kippenberg, Nat. Phys.**4**, 415 (2008).
[9] S. Gröblacher, J. B. Hertzberg, M. R. Vanner, G. D. Cole, S. Gigan, K. C. Schwab, and M. Aspelmeyer, Nat. Phys. **5**, 485 (2009).
[10] Y.-S. Park and H. Wang, Nat. Phys. **5**, 489 (2009).
[11] A. Schliesser, O. Arcizet, R. Rivère, G. Anetsberger, and T. J. Kippenberg, Nat. Phys. **5**, 509 (2009).
[12] T. Rocheleau, T. Ndukum, C. Macklin, J. B. Hertzberg, A. A. Clerk, and K. C. Schwab, Nature (London) **463**, 72 (2010).
[13] I. Wilson-Rae, N. Nooshi, W. Zwerger, and T. J. Kippenberg, Phys. Rev. Lett. **99**, 093901 (2007).
[14] F. Marquardt, J. P. Chen, A. A. Clerk, and S. M. Girvin, Phys. Rev. Lett. **99**, 093902 (2007).
[15] C. Genes, D. Vitali, P. Tombesi, S. Gigan, and M. Aspelmeyer, Phys. Rev. A **77**, 033804 (2008).
[16] J. B. Hertzberg, T. Rocheleau, T. Ndukum, M. Savva, A. A. Clerk, and K. C. Schwab, Nat. Phys. **6**, 213 (2010).
[17] M. R. Vanner, I. Pikovski, G. D. Cole, M. S. Kim, Č. Brukner, K. Hammerer, G. J. Milburn, and M. Aspelmeyer, Proc. Natl. Acad. Sci. U.S.A. **108**, 16182 (2011).
[18] V. B. Braginsky, Yu. I. Vorontsov, and F. Ya. Khalili, JETP Lett. **27**, 276 (1978).
[19] V. B. Braginsky, *Quantum Measurements* (Cambridge University Press, Cambridge, U.K., 1978).
[20] S. Gröblacher, K. Hammerer, M. R. Vanner, and M. Aspelmeyer, Nature (London) **460**, 724 (2009).
[21] T. A. Palomaki, J. W. Harlow, J. D. Teufel, R. W. Simmonds, and K. W. Lehnert, Nature (London) **495**, 210 (2013).
[22] J. M. Dobrindt, I. Wilson-Rae, and T. J. Kippenberg, Phys. Rev. Lett. **101**, 263602 (2008).
[23] S. Huang and G. S. Agarwal, Phys. Rev. A **80**, 033807 (2009).
[24] U. Akram, N. Kiesel, M. Aspelmeyer, and G. J. Milburn, New J. Phys. **12**, 083030 (2010).
[25] A. D. O'Connell *et al.*, Nature (London) **464**, 697 (2010).
[26] J. M. Taylor, A. S. Sørensen, C. M. Marcus, and E. S. Polzik, Phys. Rev. Lett. **107**, 273601 (2011).
[27] I. Wilson-Rae, N. Nooshi, J. Dobrindt, T. J. Kippenberg, and W. Zwerger, New J. Phys. **10**, 095007 (2008).
[28] P. Rabl, C. Genes, K. Hammerer, and M. Aspelmeyer, Phys. Rev. A **80**, 063819 (2009).
[29] C. K. Law, Phys. Rev. A **51**, 2537 (1995).
[30] R. Ghobadi, A. R. Bahrampour, and C. Simon, Phys. Rev. A **84**, 033846 (2011).
[31] See Supplemental Material at http://link.aps.org/supplemental/10.1103/PhysRevLett.110.153606 for more details.
[32] Q. Xu, P. Dong, and M. Lipson, Nat. Phys. **3**, 406 (2007).
[33] K. Kondo, M. Shinkawa, Y. Hamachi, Y. Saito, Y. Arita, and T. Baba, Phys. Rev. Lett. **110**, 053902 (2013).
[34] R. A. Soref and B. R. Bennett, IEEE J. Quantum Electron. **23**, 123 (1987).
[35] I. Favero and K. Karrai, New J. Phys. **10**, 095006 (2008).
[36] L. Tian, Phys. Rev. B **79**, 193407 (2009).
[37] Y. Li, L.-A. Wu, and Z. D. Wang, Phys. Rev. A **83**, 043804 (2011).
[38] J.-Q. Liao and C. K. Law, Phys. Rev. A **84**, 053838 (2011).
[39] X. Wang, S. Vinjanampathy, F. W. Strauch, and K. Jacobs, Phys. Rev. Lett. **107**, 177204 (2011).
[40] S. Machnes, J. Cerrillo, M. Aspelmeyer, W. Wieczorek, M. B. Plenio, and A. Retzker, Phys. Rev. Lett. **108**, 153601 (2012).
[41] C. Genes, H. Ritsch, and D. Vitali, Phys. Rev. A **80**, 061803(R) (2009).
[42] J. Restrepo, J. Gabelli, C. Ciuti, and I. Favero, C.R. Physique **12**, 860 (2011).
[43] S. De Liberato, N. Lambert, and F. Nori, Phys. Rev. A **83**, 033809 (2011).
[44] F. Elste, S. M. Girvin, and A. A. Clerk, Phys. Rev. Lett. **102**, 207209 (2009).
[45] A. Xuereb, R. Schnabel, and K. Hammerer, Phys. Rev. Lett. **107**, 213604 (2011).
[46] M. Li, W. H. P. Pernice, and H. X. Tang, Phys. Rev. Lett. **103**, 223901 (2009).

Supplementary Material for: Dynamic dissipative cooling of a mechanical oscillator in strong-coupling optomechanics

Yong-Chun Liu[1,2], Yun-Feng Xiao[1],* Xingsheng Luan[2], and Chee Wei Wong[2†]
[1]*State Key Laboratory for Mesoscopic Physics and School of Physics, Peking University, Beijing 100871, P. R. China and*
[2]*Optical Nanostructures Laboratory, Columbia University, New York, NY 10027, USA*
(Dated: March 13, 2013)

This Supplementary Material is organized as follows. In Sec. I, we present the linearization of the optomechanical Hamiltonian. Using the quantum master equation, we describe the covariance approach to calculate the mean phonon number in Sec. II. With this approach, we derive the steady-state cooling limit in Sec. III and the time evolution of mean phonon number in Sec. IV. In Sec. V, we calculate the instantaneous-state cooling limit in the strong coupling regime and optimize the result according to the frequency matching condition. In Sec. VI, the dynamic modulation of cavity dissipation is introduced. In Sec. VII, we discuss the dissipation quantum backaction and interaction quantum backaction. In Sec. VIII we investigate the effect of dissipation pulsewidth. The discussion on the bad-cavity limit is studied in Sec. IX.

I. LINEARIZED OPTOMECHANICAL HAMILTONIAN

The optomechanical Hamiltonian with one optical mode coupled to one mechanical mode is given by [1]

$$H=-\Delta a^{\dagger}a+\omega_{\rm m}b^{\dagger}b+ga^{\dagger}a(b+b^{\dagger})+(\Omega a^{\dagger}+\Omega^{*}a), \tag{1}$$

where we work in the frame rotating at the input laser frequency ω. Here $\Delta=\omega-\omega_{\rm c}$ is the input-cavity detuning, a (b) is the annihilation operator of the optical (mechanical) mode with $\omega_{\rm c}$ ($\omega_{\rm m}$) being the corresponding angular resonance frequency; g represents the single-photon optomechanical coupling rate; $\Omega=\sqrt{\kappa_{\rm ex}P/(\hbar\omega)}e^{i\phi}$ denotes the driving strength, where P is the input laser power, ϕ is the initial phase of the input laser and $\kappa_{\rm ex}$ is the input-cavity coupling rate.

The quantum Langevin equations are given by

$$\dot{a}=\left(i\Delta-\frac{\kappa}{2}\right)a-iga(b+b^{\dagger})-i\Omega-\sqrt{\kappa_{\rm ex}}a_{\rm in,ex}-\sqrt{\kappa_0}a_{\rm in,0}, \tag{2a}$$

$$\dot{b}=\left(-i\omega_{\rm m}-\frac{\gamma}{2}\right)b-iga^{\dagger}a-\sqrt{\gamma}b_{\rm in}, \tag{2b}$$

where κ_0 is the intrinsic cavity dissipation rate; $\kappa=\kappa_0+\kappa_{\rm ex}$ is the total cavity dissipation rate; γ is the dissipation rate of the mechanical mode; $a_{\rm in,0}$, $a_{\rm in,ex}$ and $b_{\rm in}$ are the noise operators associated with the intrinsic cavity dissipation, external cavity dissipation (input-cavity coupling) and mechanical dissipation, respectively.

Coherent laser input results in the displacements of both the optical and mechanical harmonic oscillators. For convenience, a displacement transformation is applied, i. e., $a\equiv a_1+\alpha$, $b\equiv b_1+\beta$, where α and β are c-numbers, denoting the displacements of the optical and mechanical modes; a_1 and b_1 are the displaced operators, representing the quantum fluctuations of the optical and mechanical modes around their classical values. By separating the classical and quantum components, the quantum Langevin equations are rewritten as

$$\dot{\alpha}=\left(i\Delta'-\frac{\kappa}{2}\right)\alpha-i\Omega, \tag{3a}$$

$$\dot{\beta}=\left(-i\omega_{\rm m}-\frac{\gamma}{2}\right)\beta-ig\left|\alpha\right|^{2}, \tag{3b}$$

$$\dot{a}_1=\left(i\Delta'-\frac{\kappa}{2}\right)a_1-ig\alpha(b_1+b_1^{\dagger})-iga_1(b_1+b_1^{\dagger})-\sqrt{\kappa_{\rm ex}}a_{\rm in,ex}-\sqrt{\kappa_0}a_{\rm in,0}, \tag{3c}$$

$$\dot{b}_1=\left(-i\omega_{\rm m}-\frac{\gamma}{2}\right)b_1-ig\left(\alpha^{*}a_1+\alpha a_1^{\dagger}\right)-iga_1^{\dagger}a_1-\sqrt{\gamma}b_{\rm in}, \tag{3d}$$

*Electronic address: yfxiao@pku.edu.cn; URL: www.phy.pku.edu.cn/∼yfxiao/index.html
†Electronic address: cww2014@columbia.edu

where the optomechanical-coupling modified detuning $\Delta' = \Delta - g(\beta + \beta^*)$. Under strong driving condition, the classical components dominate and the nonlinear terms $iga_1(b_1 + b_1^\dagger)$ and $iga_1^\dagger a_1$ in Eqs. (3c) and (3d) can be neglected, respectively. Then we obtain the linearized Hamiltonian $H_L = -\Delta' a_1^\dagger a_1 + \omega_{\rm m} b_1^\dagger b_1 + (Ga_1^\dagger + G^* a_1)(b_1 + b_1^\dagger)$ (Eq. (1) of the main text), where $G = \alpha g$ is the linearized optomechanical coupling strength.

II. CALCULATION OF MEAN PHONON NUMBER

With the linearized Hamiltonian, the quantum master equation reads

$$\begin{aligned}\dot{\rho} = {} & i[\rho, -\Delta' a_1^\dagger a_1 + \omega_{\rm m} b_1^\dagger b_1 + (Ga_1^\dagger + G^* a_1)(b_1 + b_1^\dagger)] \\ & + \frac{\kappa}{2}\left(2a_1\rho a_1^\dagger - a_1^\dagger a_1\rho - \rho a_1^\dagger a_1\right) + \frac{\gamma}{2}(n_{\rm th}+1)\left(2b_1\rho b_1^\dagger - b_1^\dagger b_1\rho - \rho b_1^\dagger b_1\right) + \frac{\gamma}{2}n_{\rm th}\left(2b_1^\dagger\rho b_1 - b_1 b_1^\dagger\rho - \rho b_1 b_1^\dagger\right), \end{aligned} \tag{4}$$

where $n_{\rm th}$ is the thermal phonon number in the environment. Since the Hamiltonian is linear, it does not mix moments with different orders. To calculate the mean phonon number, it is not necessary to calculate all the matrix elements of the density operator ρ, instead we need to determine the mean values of all the second-order moments, $\bar{N}_a = \langle a_1^\dagger a_1\rangle$, $\bar{N}_b = \langle b_1^\dagger b_1\rangle$, $\langle a_1^\dagger b_1\rangle$, $\langle a_1 b_1\rangle$, $\langle a_1^2\rangle$ and $\langle b_1^2\rangle$. The differential equations are given by

$$\frac{d}{dt}\bar{N}_a = -i\left(G\langle a_1^\dagger b_1\rangle - G^*\langle a_1^\dagger b_1\rangle^* + G\langle a_1 b_1\rangle^* - G^*\langle a_1 b_1\rangle\right) - \kappa\bar{N}_a, \tag{5a}$$

$$\frac{d}{dt}\bar{N}_b = -i\left(-G\langle a_1^\dagger b_1\rangle + G^*\langle a_1^\dagger b_1\rangle^* + G\langle a_1 b_1\rangle^* - G^*\langle a_1 b_1\rangle\right) - \gamma\bar{N}_b + \gamma n_{\rm th}, \tag{5b}$$

$$\frac{d}{dt}\langle a_1^\dagger b_1\rangle = [-i(\Delta + \omega_{\rm m}) - \frac{\kappa+\gamma}{2}]\langle a_1^\dagger b_1\rangle - i\left(G^*\bar{N}_a - G^*\bar{N}_b + G\langle a_1^2\rangle^* - G^*\langle b_1^2\rangle\right), \tag{5c}$$

$$\frac{d}{dt}\langle a_1 b_1\rangle = [i(\Delta - \omega_{\rm m}) - \frac{\kappa+\gamma}{2}]\langle a_1 b_1\rangle - i\left(G\bar{N}_a + G\bar{N}_b + G + G^*\langle a_1^2\rangle + G\langle b_1^2\rangle\right), \tag{5d}$$

$$\frac{d}{dt}\langle a_1^2\rangle = (2i\Delta - \kappa)\langle a_1^2\rangle - 2iG\left(\langle a_1 b_1\rangle + \langle a_1^\dagger b_1\rangle^*\right), \tag{5e}$$

$$\frac{d}{dt}\langle b_1^2\rangle = (-2i\omega_{\rm m} - \gamma)\langle b_1^2\rangle - 2i\left(G^*\langle a_1 b_1\rangle + G\langle a_1^\dagger b_1\rangle\right). \tag{5f}$$

These equations can also be found in Ref. [2], where the steady-state covariance matrix is used to obtain the final occupancy of the mechanical resonator. Note that in the above calculation, cut-off of the density matrix is not necessary and the solutions are exact.

III. STEADY-STATE COOLING LIMIT

In the stable regime, which requires $|G|^2 < -(4\Delta'^2 + \kappa^2)\omega_{\rm m}/(16\Delta')$ for red detuning $\Delta' < 0$ [3], the system finally reaches the steady state, and the derivatives in Eq. (5) all become zero. Then the second-order moments in the steady state satisfy a set of algebraic equations. Under the condition $\Delta' = -\omega_{\rm m}$ and cooperativity $C \equiv 4|G|^2/(\gamma\kappa) \gg 1$, we obtain the final phonon occupancy

$$\bar{N}_{\rm std} \simeq \frac{4|G|^2 + \kappa^2}{4|G|^2(\kappa+\gamma)}\gamma n_{\rm th} + \frac{4\omega_{\rm m}^2\left(\kappa^2 + 8|G|^2\right) + \kappa^2\left(\kappa^2 - 8|G|^2\right)}{16\omega_{\rm m}^2(4\omega_{\rm m}^2 + \kappa^2 - 16|G|^2)}. \tag{6}$$

Here the first term, being proportional to the environmental thermal phonon number $n_{\rm th}$, is the classical cooling limit; the second term, which does not depend on $n_{\rm th}$, corresponds to the quantum cooling limit. In the resolved sideband case, Eq. (6) reduces to Eq. (2) of the main text. Note that Ref. [2] and Ref. [4] present similar results in the strong coupling regime, with the quantum cooling limit $|G|^2/(2\omega_{\rm m}^2)$. In our calculations we find that the term $\omega_{\rm m}^2 - 4|G|^2$ in the denominator cannot be simplified to be $\omega_{\rm m}^2$ for relatively strong coupling strength $|G|$. Therefore, a more exact quantum cooling limit is $|G|^2/[2(\omega_{\rm m}^2 - 4|G|^2)]$, which also indicates that the stable condition $2|G| < \omega_{\rm m}$ should be satisfied.

IV. TIME EVOLUTION OF MEAN PHONON NUMBER

The steady-state solutions do not provide full information of the cooling process. Here we directly solve the differential equations Eq. (5) to obtain the time evolution of mean phonon number. For arbitrary parameters, Eq. (5) can be solved numerically. Especially, under the conditions (1) resolved sideband, (2) $\Delta' = -\omega_{\rm m}$, (3) $C \gg 1$, simple analytical expressions are available for the weak coupling and strong coupling regimes. In the weak coupling regime, using the approximation $\sqrt{16\left|G\right|^2-\kappa^2} \simeq i\kappa$, we obtain

$$\bar{N}_b^{\rm wk} \simeq \frac{(\gamma+\Gamma e^{-\Gamma t})}{\gamma+\Gamma} n_{\rm th} + \frac{\kappa^2}{16\omega_{\rm m}^2}\left(1-e^{-\Gamma t}\right), \tag{7}$$

where $\Gamma = 4|G|^2/\kappa$ is the cooling rate. In this case the cooling process corresponds to the exponential decay (with cooling rate Γ) of the mean phonon number from $n_{\rm th}$ to the steady-state cooling limit $\bar{N}_{\rm std}^{\rm wk} \simeq \gamma n_{\rm th}/(\Gamma+\gamma)+\kappa^2/(16\omega_{\rm m}^2)$.

In the strong coupling regime, to obtain analytical results, it is more convenient to calculate the contribution of the rotating-wave terms $Ga_1^\dagger b_1 + G^* a_1 b_1^\dagger$ and counter-rotating-wave terms $Ga_1^\dagger b_1^\dagger + G^* a_1 b_1$ separately. First, in Eq. (5) the counter-rotating interactions are neglected, then the mean phonon number is obtained as

$$\bar{N}_{b,1}^{\rm str} \simeq n_{\rm th}\frac{\gamma+\frac{1}{2}e^{-\frac{\kappa+\gamma}{2}t}\left[\kappa-\gamma+(\kappa+\gamma)\cos(\omega_+-\omega_-)t\right]}{\kappa+\gamma}, \tag{8}$$

where

$$\omega_\pm = \sqrt{\omega_{\rm m}^2 \pm 2\left|G\right|\omega_{\rm m}} \tag{9}$$

are the eigenfrequencies of the normal modes. This term $\bar{N}_{b,1}^{\rm str}$ is proportional to the environmental thermal phonon number $n_{\rm th}$ and behaves as a decaying Rabi oscillation, corresponding to the beam-splitter interaction $a_1^\dagger b_1 + a_1 b_1^\dagger$. Next, taking the counter-rotating terms into account and setting $n_{\rm th} = 0$, we obtain the contribution of quantum backaction as

$$\bar{N}_{b,2}^{\rm str} \simeq \frac{\left|G\right|^2\left[1-e^{-\frac{\kappa+\gamma}{2}t}\cos(\omega_++\omega_-)t\cos(\omega_+-\omega_-)t\right]}{2(\omega_{\rm m}^2-4\left|G\right|^2)}. \tag{10}$$

Note that $\bar{N}_{b,2}^{\rm str}$ does not depend on $n_{\rm th}$, corresponding to the vacuum fluctuation-induced heating. For $t\to\infty$, $\bar{N}_{b,2}^{\rm str} \to \left|G\right|^2/[2(\omega_{\rm m}^2-4\left|G\right|^2)]$, which is just the steady-state quantum cooling limit. With Eqs. (8) and (10), the time evolution of the mean phonon number in the strong coupling regime is given by $\bar{N}_b^{\rm str} = \bar{N}_{b,1}^{\rm str} + \bar{N}_{b,2}^{\rm str}$ (Eq. (3) of the main text).

V. INSTANTANEOUS-STATE COOLING LIMIT AND FREQUENCY MATCHING

The minimum value of $\bar{N}_{b,1}^{\rm str}$ is obtained when $t \simeq \pi/(\omega_+-\omega_-)$ (half Rabi oscillation cycle), yielding $\cos(\omega_+-\omega_-)t \simeq -1$ and

$$\bar{N}_{b,1}^{\rm str}\,|_{\rm min} \simeq \frac{\gamma n_{\rm th}}{\kappa}\left(1-e^{-\frac{\kappa+\gamma}{2}\frac{\pi}{\omega_+-\omega_-}}\right) \simeq \frac{\pi\gamma n_{\rm th}}{4\left|G\right|}. \tag{11}$$

The minimum value of $\bar{N}_{b,2}^{\rm str}$ depends on the carrier-envelope frequency matching, where the carrier frequency is $\omega_+ + \omega_-$ and the envelope frequency is $\omega_+ - \omega_-$. The frequency matching condition is

$$\frac{\omega_+ + \omega_-}{\omega_+ - \omega_-} = k, \tag{12}$$

where $k = 3, 5...$ In this case when $t = \pi/(\omega_+ - \omega_-)$, we have $\cos(\omega_+ + \omega_-)t = \cos k\pi = -1$, and

$$\bar{N}_{b,2}^{\rm str}\,|_{\rm min}^{\rm opt} \simeq \frac{\left|G\right|^2}{2(\omega_{\rm m}^2-4\left|G\right|^2)}\left(1-e^{-\frac{\kappa+\gamma}{2}\frac{\pi}{\omega_+-\omega_-}}\right) \simeq \frac{\pi\kappa|G|}{8(\omega_{\rm m}^2-4|G|^2)}. \tag{13}$$

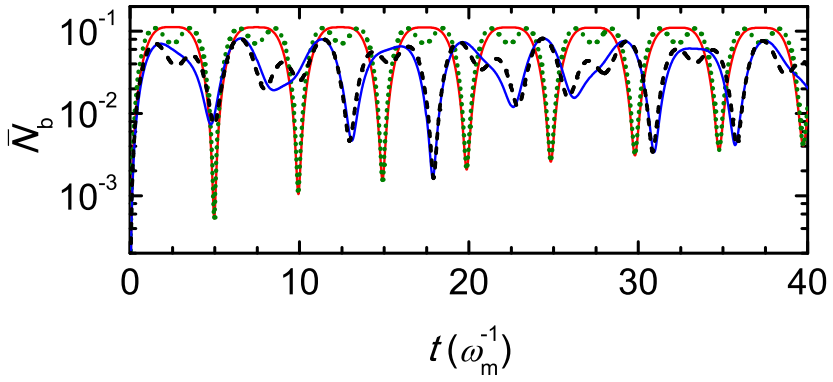

FIG. S1: (color online) (a) Time evolution of $\bar{N}_b$ for $n_{\rm th}=0$, $G/\omega_{\rm m}=0.25$ (black dashed curve) and 0.3 (green dotted curve). The blue and red solid curves are the corresponding analytical results given by Eq. (10). Other parameters are $\kappa/\omega_{\rm m}=0.003$ and $\gamma/\omega_{\rm m}=10^{-5}$.

If the frequency matching condition Eq. (12) is not satisfied, The minimum value of $\bar{N}_{b,2}^{\rm str}$ is obtained when $t\simeq 2\pi/(\omega_+ +\omega_-)$, which yields $\cos(\omega_+ +\omega_-)t\simeq 1$, and

$$\cos(\omega_+ -\omega_-)t\simeq\cos 2\pi\frac{\omega_+ -\omega_-}{\omega_+ +\omega_-}\simeq 1-2(\pi\frac{\omega_+ -\omega_-}{\omega_+ +\omega_-})^2\simeq 1-\frac{2\pi^2|G|^2}{\omega_{\rm m}^2-|G|^2}. \tag{14}$$

Thus we obtain

$$\bar{N}_{b,2}^{\rm str}|_{\rm min}\simeq\frac{|G|^2}{2(\omega_{\rm m}^2-4\,|G|^2)}\times\frac{2\pi^2|G|^2}{\omega_{\rm m}^2-|G|^2}=\frac{\pi^2\,|G|^4}{(\omega_{\rm m}^2-|G|^2)(\omega_{\rm m}^2-4\,|G|^2)}. \tag{15}$$

In the main text, the instantaneous-state cooling limits Eqs. (4) and (5) are from the above expressions.

To verify the optimized instantaneous-state cooling limit, in Fig. S1 we plot the time evolution of phonon occupation starting from $n_{\rm th}=0$ for $G/\omega_{\rm m}=0.25$ and 0.3. It shows explicitly that when $G/\omega_{\rm m}=0.3$, the carrier-envelope frequencies match, leading to minimum phonon occupancy less than 10^{-3}; while without matching ($G/\omega_{\rm m}=0.25$) the minimum phonon number is still 10^{-2} at the first Rabi oscillation cycle. We note that the numerical results agree well with the analytical expressions.

VI. DYNAMIC MODULATION OF CAVITY DISSIPATION

In the above calculations, all the parameters are time-independent. Now we introduce time-dependent cavity dissipation $\kappa(t)$. In this case the master equation (4) and the differential equations (5) still hold. We numerically solve Eqs. (5) to obtain the cooling dynamics, with the main results presented in the main text.

During the modulation of cavity dissipation $\kappa(t)$, we have assumed that the intracavity field α and thus the coupling strength G keeps time-invariant. This can be satisfied by simultaneously modulating the driving strength $\Omega(t)$. From Eqs. (3a) and (3b) we observe that this requires

$$\frac{\Omega(t)}{\Omega(0)}=\frac{i\left(\Delta'+\frac{2|G|^2}{\omega_{\rm m}}\right)-\frac{\kappa(t)}{2}}{i\left(\Delta'+\frac{2|G|^2}{\omega_{\rm m}}\right)-\frac{\kappa(0)}{2}}. \tag{16}$$

Using $\Omega(t)=\sqrt{\kappa_{\rm ex}(t)P(t)/(\hbar\omega)}e^{i\phi(t)}$ the condition reads

$$\sqrt{\frac{\kappa_{\rm ex}(t)P(t)}{\kappa_{\rm ex}(0)P(0)}}e^{i[\phi(t)-\phi(0)]}=\frac{i\left(\Delta'+\frac{2|G|^2}{\omega_{\rm m}}\right)-\frac{\kappa(t)}{2}}{i\left(\Delta'+\frac{2|G|^2}{\omega_{\rm m}}\right)-\frac{\kappa(0)}{2}}. \tag{17}$$

Note that in Eqs. (5) only the total cavity dissipation $\kappa(t)$ appear explicitly. In principle both the modulation of the internal cavity dissipation $\kappa_0(t)$ and the external cavity dissipation $\kappa_{\rm ex}(t)$ leads to the same results as long as Eq. (17) is satisfied. The difference is that the modulation of $\kappa_{\rm ex}(t)$ also changes the light intensity coupled into the cavity.

VII. DISSIPATION QUANTUM BACKACTION AND INTERACTION QUANTUM BACKACTION

In the strong coupling regime, quantum backaction behaves quite different from that in the weak coupling regime. This is because in these two regimes the dominant quantum backaction has distinct origins. In the weak coupling regime, the dominant quantum backaction stems from the added noise which accompanies with the system dissipation, which is a fundamental consequence of the fluctuation-dissipation theorem. This dissipation quantum backaction (DQBA) results in the quantum cooling limit $\kappa^2/(16\omega_{\rm m}^2)$. However, in the strong coupling regime, since the optomechanical interaction dominates over the cavity dissipation, the major contribution is the interaction quantum backaction (IQBA), which leads to the final phonon occupancy $|G|^2/[2(\omega_{\rm m}^2-4|G|^2)]$.

The IQBA is a result of strong counter-rotating interaction. For convenience, let us transform to the normal mode basis, with the relation

$$\begin{pmatrix} a_1 \\ b_1 \\ a_1^\dagger \\ b_1^\dagger \end{pmatrix} = \begin{pmatrix} \eta_{++} & \eta_{-+} & \eta_{+-} & \eta_{--} \\ \eta_{++} & -\eta_{-+} & \eta_{+-} & -\eta_{--} \\ \eta_{+-} & \eta_{--} & \eta_{++} & \eta_{-+} \\ \eta_{+-} & -\eta_{--} & \eta_{++} & -\eta_{-+} \end{pmatrix} \begin{pmatrix} c_+ \\ c_- \\ c_+^\dagger \\ c_-^\dagger \end{pmatrix}, \tag{18}$$

where $c_\pm$ are the eigenmodes with the corresponding eigenfrequencies $\omega_\pm = \sqrt{\omega_{\rm m}^2 \pm 2|G|\omega_{\rm m}}$, and the coefficients

$$\eta_{++} = \frac{1}{2\sqrt{2}}\left(\sqrt{\frac{\omega_{\rm m}}{\omega_+}} + \sqrt{\frac{\omega_+}{\omega_{\rm m}}}\right), \tag{19a}$$

$$\eta_{+-} = \frac{1}{2\sqrt{2}}\left(\sqrt{\frac{\omega_{\rm m}}{\omega_+}} - \sqrt{\frac{\omega_+}{\omega_{\rm m}}}\right), \tag{19b}$$

$$\eta_{-+} = \frac{1}{2\sqrt{2}}\left(\sqrt{\frac{\omega_{\rm m}}{\omega_-}} + \sqrt{\frac{\omega_-}{\omega_{\rm m}}}\right), \tag{19c}$$

$$\eta_{--} = \frac{1}{2\sqrt{2}}\left(\sqrt{\frac{\omega_{\rm m}}{\omega_-}} - \sqrt{\frac{\omega_-}{\omega_{\rm m}}}\right). \tag{19d}$$

It is clear that due to the counter-rotating interaction, the annihilation operators of the eigenmodes are mixtures of the annihilation operators and creation operators of the photon and phonon modes. The degree of mixing is characterized by η_{+-} and η_{--}. A large interaction strength $|G|$ leads to large mode splitting and thereby results in a strong degree of mixing. The final phonon occupancy is roughly proportional to $\eta_{+-}^2+\eta_{--}^2$, which scale as $|G|^2/\omega_{\rm m}^2$.

VIII. EFFECT OF DISSIPATION PULSEWIDTH

The dissipation pulse suppresses the IQBA, while the DQBA is enhanced due to added noise accompanying with the increased dissipation. Thus it is important to optimize the pulse duration. In Fig. S2 we plot the time evolution of mean phonon number under single-pulse modulation with different pulsewidths $T_{\rm p}=0.1T_{\rm R}$, $T_{\rm R}$, $5T_{\rm R}$ and infinity, where $T_{\rm R}=\pi/(2|G|)$ is the half Rabi oscillation cycle. The parameters are the same as that in Figs. 2(c) and (d) of the main text except for the pulsewidths. It shows that within the pulse duration, the phonon number increases gradually, which is the effect of dissipation quantum backaction. To analyze this explicitly, let us consider the case of an infinitely-long dissipation pulse applied from $t=0$, which corresponds to highly unresolved sideband case with cavity dissipation $\kappa_{\rm inf} \gg \omega_{\rm m}$. Using the quantum noise approach, the rate for absorbing and emitting a phonon by the cavity field are respectively given by

$$A_- = \frac{G^2\kappa_{\rm inf}}{\left(\omega_{\rm m}+\Delta'\right)^2+\left(\frac{\kappa_{\rm inf}}{2}\right)^2}, \tag{20a}$$

$$A_+ = \frac{G^2\kappa_{\rm inf}}{\left(\omega_{\rm m}-\Delta'\right)^2+\left(\frac{\kappa_{\rm inf}}{2}\right)^2}. \tag{20b}$$

With detuning $\Delta'=-\omega_{\rm m}$, the net optical damping rate is given by

$$\begin{aligned}\Gamma_{\rm inf} = A_- - A_+ &= \frac{4G^2}{\kappa_{\rm inf}} - \frac{G^2\kappa_{\rm inf}}{\left(2\omega_{\rm m}\right)^2+\left(\frac{\kappa_{\rm inf}}{2}\right)^2} \\ &\simeq \frac{4G^2}{\kappa_{\rm inf}}\left(\frac{4\omega_{\rm m}}{\kappa_{\rm inf}}\right)^2 = \frac{C\gamma}{R},\end{aligned} \tag{21}$$

where we have introduced the resolved sideband parameter $R \equiv \kappa_{\rm inf}^2/(16\omega_{\rm m}^2)$. The final phonon occupancy is calculated as

$$n_{\rm inf} = n_{\rm inf}^{\rm c} + n_{\rm inf}^{\rm q}, \tag{22a}$$

$$n_{\rm inf}^{\rm c} = \frac{\gamma n_{\rm th}}{\gamma + \Gamma_{\rm inf}} \simeq \frac{R n_{\rm th}}{R + C}, \tag{22b}$$

$$n_{\rm inf}^{\rm q} = \frac{A_+}{\gamma + \Gamma_{\rm inf}} \simeq \frac{RC}{R + C} = \frac{4G^2\kappa_{\rm inf}^2}{64G^2\omega_{\rm m}^2 + \gamma\kappa_{\rm inf}^3}. \tag{22c}$$

Note that the results in the resolved sideband (RSB) case are different, which read [5, 6]

$$A_-^{\rm RSB} \simeq \frac{4G^2}{\kappa} = C\gamma, \tag{23a}$$

$$A_+^{\rm RSB} \simeq \frac{G^2\kappa}{4{\omega_{\rm m}}^2} = RC\gamma, \tag{23b}$$

$$\Gamma_{\rm RSB} \simeq \frac{4G^2}{\kappa} = C\gamma, \tag{23c}$$

$$n_{\rm RSB} = n_{\rm RSB}^{\rm c} + n_{\rm RSB}^{\rm q}, \tag{23d}$$

$$n_{\rm RSB}^{\rm c} \simeq \frac{\gamma n_{\rm th}}{\Gamma_{\rm RSB}} \simeq \frac{n_{\rm th}}{C}, \tag{23e}$$

$$n_{\rm RSB}^{\rm q} \simeq \frac{A_+}{\Gamma_{\rm RSB}} \simeq R. \tag{23f}$$

Here $A_-^{\rm RSB} \gg A_+^{\rm RSB}$, thus $A_+^{\rm RSB}$ can be neglected, resulting in the large net optical damping rate $\Gamma_{\rm RSB}$. However, for

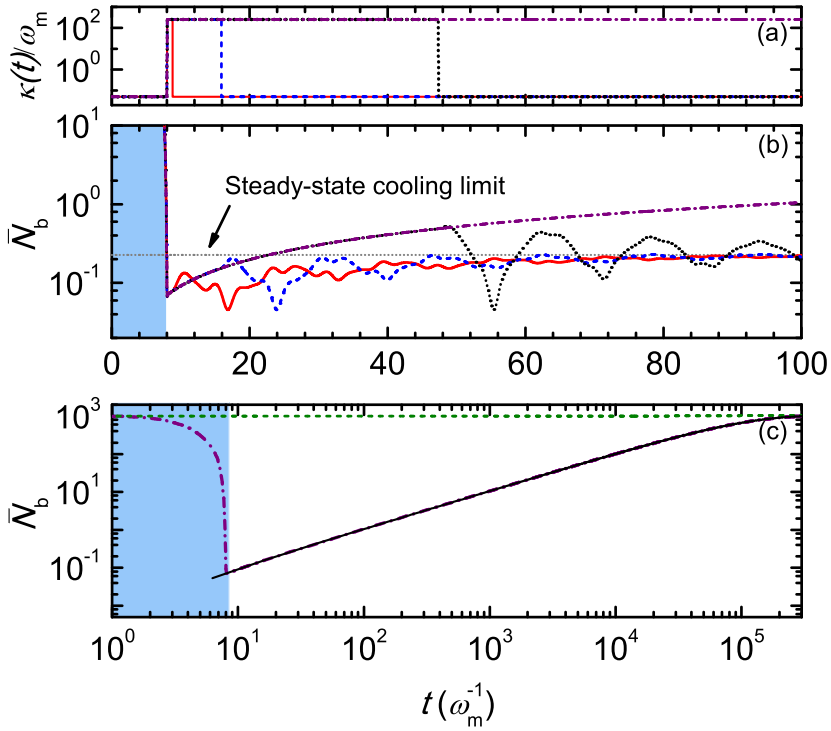

FIG. S2: (color online) (a) Modulation scheme of the cavity dissipation and (b) time evolution of mean phonon number $\bar{N}_b$ under single-pulse modulation for pulsewidth: $0.1T_{\rm R}$ (red solid curve), $T_{\rm R}$ (blue dashed curve), $5T_{\rm R}$ (black dotted curve), infinity (purple dashed-dotted curve). In (b), the dotted horizontal line corresponds to the steady-state cooling limit; the vertical coordinate range from 10 to 10^3 is not shown. (c) Logarithmic-logarithmic plot of $\bar{N}_b$ under single-pulse modulation with infinitely-long pulsewidth applied at $t = T_{\rm R}$ (purple dashed-dotted curve). The black solid curve denotes the analytical results given by Eq. (24) with $n(T_{\rm R}) = 0.07$. The green dashed curve is a comparison with infinitely-long dissipation pulse applied from $t = 0$. Other parameters: $n_{\rm th} = 10^3$, $\gamma/\omega_{\rm m} = 10^{-5}$, $\kappa/\omega_{\rm m} = 0.05$, $G/\omega_{\rm m} = 0.2$.

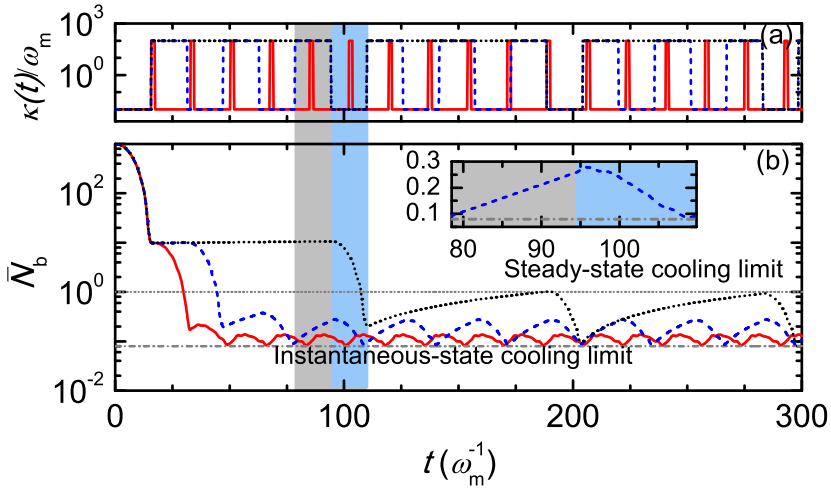

FIG. S3: (color online) (a) Modulation scheme of the cavity dissipation and (b) time evolution of mean phonon number $\bar{N}_b$ under periodic modulation for pulsewidth: $0.1T_R$ (red solid curve), T_R (blue dashed curve), $5T_R$ (black dotted curve). In (b), the dotted (dashed-dotted) horizontal line corresponds to the steady-state (instantaneous-state) cooling limit. The inset is a zoom in linear vertical coordinate view of the shaded region in (b) for T_R pulsewidth, where the gray shaded region illustrates the region of high dissipation (and high dissipation backaction) while the blue shaded region is that of low dissipation. The non-monotonic decay in the blue shaded region is due to residual interaction backaction. Other parameters: $n_{th} = 10^3$, $\gamma/\omega_m = 10^{-5}$, $\kappa/\omega_m = 0.01$, $G/\omega_m = 0.1$.

the highly unresolved sideband case, A_- and A_+ are nearly equal, leading to a small net optical damping rate Γ_{inf}. Furthermore, when calculating the final phonon occupancy, the intrinsic mechanical damping rate γ is negligible in the resolved sideband limit since $\Gamma_{RSB} \gg \gamma$. But in the highly unresolved sideband limit γ cannot be neglected since it could even be larger than the net optical damping rate Γ_{inf}. Considering a specific example, $n_{th} = 10^3$, $\gamma/\omega_m = 10^{-5}$, $\kappa_{inf}/\omega_m = 250$, $G/\omega_m = 0.2$, we obtain $C = 64$, $R = 3906$, yielding $\Gamma_{inf}/\gamma = 0.016$, $n_{inf}^c = 984$, $n_{inf}^q = 63$ and $n_{inf} = 1047$.

We are interested in the time evolution of the mean phonon number with given phonon occupancy at $t = t_0$ in this highly unresolved sideband regime. With the above results, we obtain

$$n(t) = n(t_0) + [n_{inf} - n(t_0)]\left[1 - e^{-(\gamma+\Gamma_{inf})(t-t_0)}\right], \tag{24}$$

$$\frac{dn(t)}{dt} = (\gamma + \Gamma_{inf})\,[n_{inf} - n(t_0)]\,e^{-(\gamma+\Gamma_{inf})(t-t_0)}. \tag{25}$$

For short time scales near $t = t_0$, we have $e^{-(\gamma+\Gamma_{inf})(t-t_0)} \simeq 1$, and $dn(t)/dt \simeq (\gamma+\Gamma_{inf})\,[n_{inf} - n(t_0)]$, which is limited by the small net optical damping rate Γ_{inf}.

In Fig. S2 (c) we plot the time evolution of the mean phonon number under a single infinitely-long dissipation pulse applied at $t = T_R$ (purple dashed-dotted curve). This corresponds to the case that the system is in the highly unresolved sideband regime from $t = T_R$. For comparison, the highly unresolved sideband case starting from $t = 0$ (green dashed curve) is also presented. It shows that, during the pulse duration, the mean phonon number increase exponentially and finally reaches the cooling limit given by Eq. (22). However, the time scale is very large due to the small total damping rate. The analytical expression given by Eq. (24) (black solid curve) is in good accordance with the numerical results. Therefore, in this highly unresolved sideband regime, since the cooling and heating have almost balanced effects, the optical field pose only insignificant effect to the mechanical resonator. When the system has been already cooled to a low-phonon-number state, it will cost a long time (compared with the pulsewidth) for the system to recover to the thermal equilibrium state.

In Fig. S3 we plot the time evolution of mean phonon number under periodic modulation with different pulsewidths $T_p = 0.1T_R$, T_R, $5T_R$. The parameter are the same as that in Fig. 3 of the main text except for the pulsewidth. It is clear that longer pulsewidth leads to the increase of the phonon number, and shorting the pulse will suppress this heating induced by the dissipation quantum backaction arising from fluctuation-dissipation. In the inset, we illustrate a zoom in view for T_R pulsewidth, where the gray (blue) shaded region illustrates the mean phonon number at the region of high (low) dissipation. With pulsewidth $T_p = 0.1T_R$ or shorter, this effect has negligible influence.

IX. DISCUSSION ON THE BAD-CAVITY LIMIT

The dynamic dissipative cooling scheme works in the strong coupling regime ($2|G| > \kappa$). Here we discuss the bad-cavity (unresolved sideband, $\kappa > \omega_{\rm m}$) case. By solving Eq. (5) with all the derivatives being zero, we obtain the generalized version of the steady-state quantum limit which holds both in the good-cavity and bad-cavity conditions

$$\bar{N}_{\rm std}^{\rm q} = \frac{\omega_{\rm m}\left(4\Delta'^2+\kappa^2\right)\left[4\left(\Delta'+\omega_{\rm m}\right)^2+\kappa^2\right]-8G^2\Delta'\left(4\Delta'^2+\kappa^2+16\Delta'\omega_{\rm m}+8\omega_{\rm m}^2\right)}{-16\Delta'\omega_{\rm m}\left[16\Delta'|G|^2+\omega_{\rm m}(4\Delta'^2+\kappa^2)\right]}, \tag{26}$$

where we have used the approximation of small mechanical decay rates γ with respect to ($\omega_{\rm m}$, κ, Δ', $|G|$).

For red detuning $\Delta' < 0$, the dynamical stability condition calculated from the Routh-Hurwitz criterion [3] is given by

$$16\Delta'|G|^2+\omega_{\rm m}(4\Delta'^2+\kappa^2) > 0, \tag{27}$$

which is also embodied in the denominator of Eq. (26). In the unresolved sideband regime, the optimal detuning to achieve the minimum fundamental cooling limit is $\Delta' = -\kappa/2$ [5, 6]. In this case Eq. (27) reduces to

$$|G| < \frac{\sqrt{\kappa\omega_{\rm m}}}{2}, \tag{28}$$

which does not satisfy the strong coupling condition. If we set $\Delta' = -\omega_{\rm m}$, the stable region requires

$$|G| < \sqrt{\frac{\omega_{\rm m}^2}{4}+\frac{\kappa^2}{16}}, \tag{29}$$

which is almost always in the weak coupling regime. One way to avoid this is to use a large detuning $\Delta' \gg \kappa$, then the stable condition reduces to

$$|G| < \frac{\sqrt{|\Delta'|\,\omega_{\rm m}}}{2}. \tag{30}$$

If $|\Delta'| > \kappa^2/\omega_{\rm m}$, strong coupling is a possibility. But in this case the detuning is so large that the cooling efficiency is very low. Therefore, in the bad-cavity limit the dynamic dissipative cooling scheme does not show special advantage.

[1] C. K. Law, Phys. Rev. A **51**, 2537 (1995).
[2] I. Wilson-Rae, N. Nooshi, J. Dobrindt, T. J. Kippenberg and W. Zwerger, New J. Phys. **10**, 095007 (2008).
[3] R. Ghobadi, A. R. Bahrampour, and C. Simon, Phys. Rev. A **84**, 033846 (2011).
[4] J. M. Dobrindt, I. Wilson-Rae, and T. J. Kippenberg, Phys. Rev. Lett. **101**, 263602 (2008).
[5] I. Wilson-Rae, N. Nooshi, W. Zwerger, and T. J. Kippenberg, Phys. Rev. Lett. **99**, 093901 (2007).
[6] F. Marquardt, J. P. Chen, A. A. Clerk, and S. M. Girvin, Phys. Rev. Lett. **99**, 093902 (2007).